JOURNAL OF AIRCRAFT
Vol. 47, No. 6, November–December 2010

Examination of Rotor Loads due to On-Blade Active Controls for Performance Enhancement

Rohit Jain*
HyPerComp, Inc., Westlake Village, California 91361
Hyeonsoo Yeo†
NASA Ames Research Center, Moffett Field, California 94035
and
Inderjit Chopra‡
University of Maryland, College Park, Maryland 20742

DOI: 10.2514/1.C000306

On-blade active controls with trailing-edge deflection, leading-edge deflection, and active-twist are studied for improvements in rotor aerodynamic efficiency and their influence on structural loads. A full-scale UH-60A Blackhawk rotor at two key flight conditions (high-speed forward flight and high-thrust forward flight) is studied using coupled computational fluid dynamics and computational structural dynamics simulations. A simulation-based trade study is carried out comprising parametric variations of geometric sizing and deployment schedules of the blade morphing. The study shows that active controls improve rotor performance and reduce rotor loads at the same time with careful selection of deployment schedule and design. In high-speed forward flight, using trailing-edge deflection, an improvement of 7.3% in performance and a reduction in the hub vibratory loads of up to 54% is achieved, and using active-twist an improvement of 7.0% in performance and up to 22% reduction in hub vibratory loads is achieved. In high-thrust forward flight, a 15.0% improvement in performance and up to 40% reduction in hub vibratory loads is achieved using leading-edge deflection.

Nomenclature

C	=	chord, in.
C_D	=	drag coefficient
C_L	=	lift coefficient
C_M	=	moment coefficient
C_T	=	rotor thrust coefficient
D_e	=	rotor effective drag, lbf
F_p	=	propulsive force, lbf
$F_{p\text{-link}}$	=	peak-to-peak magnitude of the pitch-link load, lbf
$F_{xy,4/rev}$	=	4/rev hub (nonrotating) vibratory in-plane force, lbf
$F_{z,4/\text{rev}}$	=	4/rev hub (nonrotating) vibratory vertical force, lbf
L	=	rotor lift, lbf
M	=	local Mach number at a blade section
M_y	=	peak-to-peak magnitude of the blade flap bending, ft-lbf
$M_{xy,4/\text{rev}}$	=	4/rev hub (nonrotating) vibratory in-plane moment, ft-lbf
M_z	=	peak-to-peak magnitude of the blade lag-bending, ft-lbf
P	=	rotor power, HP
q	=	freestream dynamic pressure, psi
R	=	rotor radius, in.
V	=	rotor forward speed, ft/s
δ	=	trailing-edge deflection, in.
θ	=	leading-edge deflection, deg
μ	=	advance ratio
σ	=	rotor solidity
ϕ	=	phase angle, deg
ψ	=	rotor azimuth angle, deg

Received 8 February 2010; revision received 10 June 2010; accepted for publication 15 June 2010.

*rkj@hypercomp.net (Corresponding Author).
†Aeroflightdynamics Directorate, U.S. Army Research, Development, and Engineering Command.
‡Department of Aerospace Engineering.

Introduction

A HELICOPTER rotor blade is exposed to a large variation in flow environment in one revolution (transonic flow on the advancing side to near-stall/stall on the retreating side). The aerodynamic loading leads to significant time-varying elastic deformations of the blade. On the advancing side, transonic aerodynamics creates large pitching moments on the outboard areas of the blade, especially at high-advance ratios. These moments lead to significant elastic twist of the blade, which alters the blade sectional angle of attack and affects the aerodynamic loads. If the drag divergence Mach number is exceeded, the aerodynamic performance of the rotor degrades due to shock-induced flow separation and wave drag penalty. On the retreating side, large pitch angles may lead to dynamic stall, especially at high-thrust conditions. A vortex is shed near the leading-edge of an airfoil which increases the lift as the vortex passes along the upper surface, but also increases moment and drag. It is a source of high-vibratory loads and defines the performance envelope of the rotor both in speed and thrust carrying capacity.

For improved aerodynamic performance (efficiency) of the helicopter rotor, it is desired that the lift-over-drag ratio of the airfoil at all blade sections be maximized. At a minimum, it is desired that the drag divergence Mach number, M_{dd}, be as high as possible to avoid the wave drag, and the maximum lift coefficient, $C_{L,\max}$, be as high as possible to delay or avoid stall. These are somewhat conflicting requirements as high-$C_{L,\max}$ is achieved with a high camber, which causes poor performance at transonic conditions. Similarly, high-performance transonic airfoils are thin with a sharp nose, but they have poor $C_{L,\max}$. The rotor blade airfoils are designed as a compromise weighing these requirements to meet the overall mission of the helicopter. At present, the rotor blade design is passive in that the airfoil shape remains unchanged both with the rotor azimuth (fast variation) and flight condition (slow variation).

In this paper, active controls [1] are studied that dynamically change the blade airfoil shape as a function of rotor azimuth in order

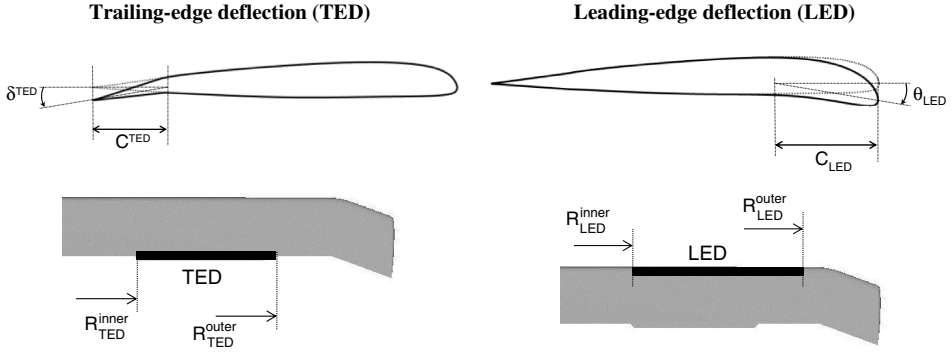

Fig. 1 TED and LED geometric parameters.

to increase the rotor aerodynamic efficiency. For dynamic shape changes, the key regions on the rotors are the advancing side, where the flow compressibility effects are important, and the retreating side, where stall effects are critical.

Several rotor performance improvement studies employing various active control-shave been reported in the literature, based on both analyses and experiments. In [2], seven active control concepts (leading-edge slat, variable leading-edge droop, oscillatory jet, Gurney flap, individual blade control, active-twist, and trailing-edge flap) have been investigated for improvement in rotor performance using comprehensive analysis. In [3], a performance improvement study has been carried out using 2/rev control inputs where a formal optimization procedure has been developed for computing the optimum set of inputs. Variable speed rotor in combination with 1/rev dynamic chord extension has been investigated in [4]. In [5], chord extension, trailing-edge flap, and Gurney flap concepts have been applied to stall-dominated flight conditions and it is shown that best gains are obtained with the chord extension concept. The analyses above were carried out using simplified aerodynamic models based on the lifting-line theory, and, typically, a free-wake representation of the rotor wake. Deflection (droop) of the leading-edge to improve performance under stalled conditions has been studied using computational fluid dynamics (CFD) in [6,7] where it is shown to be quite effective in mitigating the stall. These studies were performed for a two-dimensional airfoil. In [8], actively controlled trailing-edge flap has been investigated for stall alleviation using a coupled CFD and computational structural dynamics (CSD) analysis. It is shown that a downward deflection of the flap, which increases the camber, is quite effective in alleviating the stall, improving the performance and reducing the vibratory loads. An experimental investigation employing the individual blade control has been reported in [9,10], where wind-tunnel tests on a full-scale BO-105 rotor for performance improvement, and vibration and blade-vortex noise reduction were carried out. A power reduction of about 5% is shown with an optimum 2/rev input. Also, it is shown that 2/rev input can have a significant effect, of the order of ±40%, on the hub vibratory loads. Recently, the individual blade control of the UH-60 rotor was studied in a wind-tunnel for performance improvement, and vibration and noise reduction. With optimum control inputs, a power reduction of up to 5% was shown along with reduction in hub loads, pitch-link loads, and noise [11]. Several experimental and analytical studies have also been reported for noise and vibration reduction involving actively controlled trailing-edge flaps [12–14] and active-twist [15,16].

CFD-based high-fidelity aerodynamic modeling of actively controlled rotors reported in the literature are quite limited and most of the analytical work reported above have been carried out using simplified aerodynamic models. In the present work, CFD-based aerodynamic models are used to study actively controlled rotor employing three different, generic blade morphing concepts: trailing-edge deflection (TED), leading-edge deflection (LED), and active-twist, for two key flight conditions: high-speed and high-thrust forward flights. A novel analysis approach using CFD–CSD coupling has been developed and shown to work efficiently in analyzing morphing rotor dynamics. Compared with lifting-line models, the CFD methods solve fully three-dimensional, unsteady, turbulent Navier–Stokes equations. They calculate airfoil aerodynamic characteristics directly, and thus do not require airfoil tables for active controls. This capability enables accurate and consistent evaluation of active control concepts.

The present authors investigated TED, LED, and active-twist for the UH-60A main rotor performance improvement using coupled simulation of CFD and CSD in [17]. The improvements in performance using each of three concepts for different flight conditions were calculated and an understanding of the aeromechanics that led to the observed performance improvement was established. This study was focused on maximization of performance with various deployment schedules while the effect of dynamic blade morphing

Table 1 UH-60A blade parameters

Parameter	Value
Number of blades	4
Radius, in.	322
Chord, in.	20.76
Thickness, % chord	9.5/9.4
Rotor disk area ft^2	2261.5
Rotor blade area, ft^2	186.9
Solidity ratio	0.0826
Blade tip sweep, aft, deg	20
Airfoils	SC1095/SC1094R8
Nominal rotor speed, Ω, rpm	258
1st torsional frequency, /rev	4.3
Pretwist, deg	−16, nonlinear

Table 2 UH-60A flight conditions [19]

Parameter	High-speed (c8534)	High-thrust (c9017)
Density, slug/ft^3	0.0020823	0.0013242
Temperature, °F	71.8	24.76
Rotor speed, rpm	258.1	255.8
Airspeed, ft/ sec	266.5	170.2
Advance ratio, μ	0.368	0.237
Blade loading, C_T/σ	0.084	0.129
Freestream Mach	0.236	0.157

Table 3 Trim condition for high-speed and high-thrust flight conditions (CFD–CSD calculations) for the baseline (no active control) rotor

Parameter	High-speed (c8534)	High-thrust (c9017)
Pitch angle, deg		
Collective, θ_0	15.4	13.4
Lateral-cyclic, θ_{1c}	1.43	2.21
Longitudinal-cyclic, θ_{1s}	−9.34	−8.77
Shaft angle a, α_s, deg	8.8	2.0

[a]Positive forward tilt.

on the structural loads was not considered. Also, the optimal deployment schedule was obtained for a fixed geometric configuration (radial span and chord width) of TED and LED.

In the present study, the focus is on the structural loads. The objective is to vary the deployment schedule as well as the geometric sizing of the control surfaces so that the performance gains obtained in the previous study are achieved, and at the same time, the structural loads are reduced or minimally penalized. From the actuator design perspective, a minimization of the control surface area is sought so that, potentially, the weight penalty associated with the actuator machinery and the actuation power can be minimized. The study is carried out using coupled CFD–CSD analysis. The use of CFD analysis is especially warranted in order to address with adequate fidelity the subtle differences in geometrical configurations in the parametric studies.

The organization of this paper is as follows. First, the morphing concepts are discussed. This is followed by a description of the CFD and CSD tools employed for this study. Next, the results for the parametric studies involving geometric sizing and deployment schedules are presented and discussed for their impact on performance and structural loads.

Active Rotor Control Concepts

Three concepts have been studied in this paper: (1) TED, (2) LED, and (3) active-twist. The deflection of trailing- and leading-edge of airfoils is very effective in varying the airfoil performance characteristics while the active-twist control can be used to azimuthally vary the structural twist to improve the lift-to-drag ratios at the blade sections. These concepts, therefore, offer a wide range of possibilities

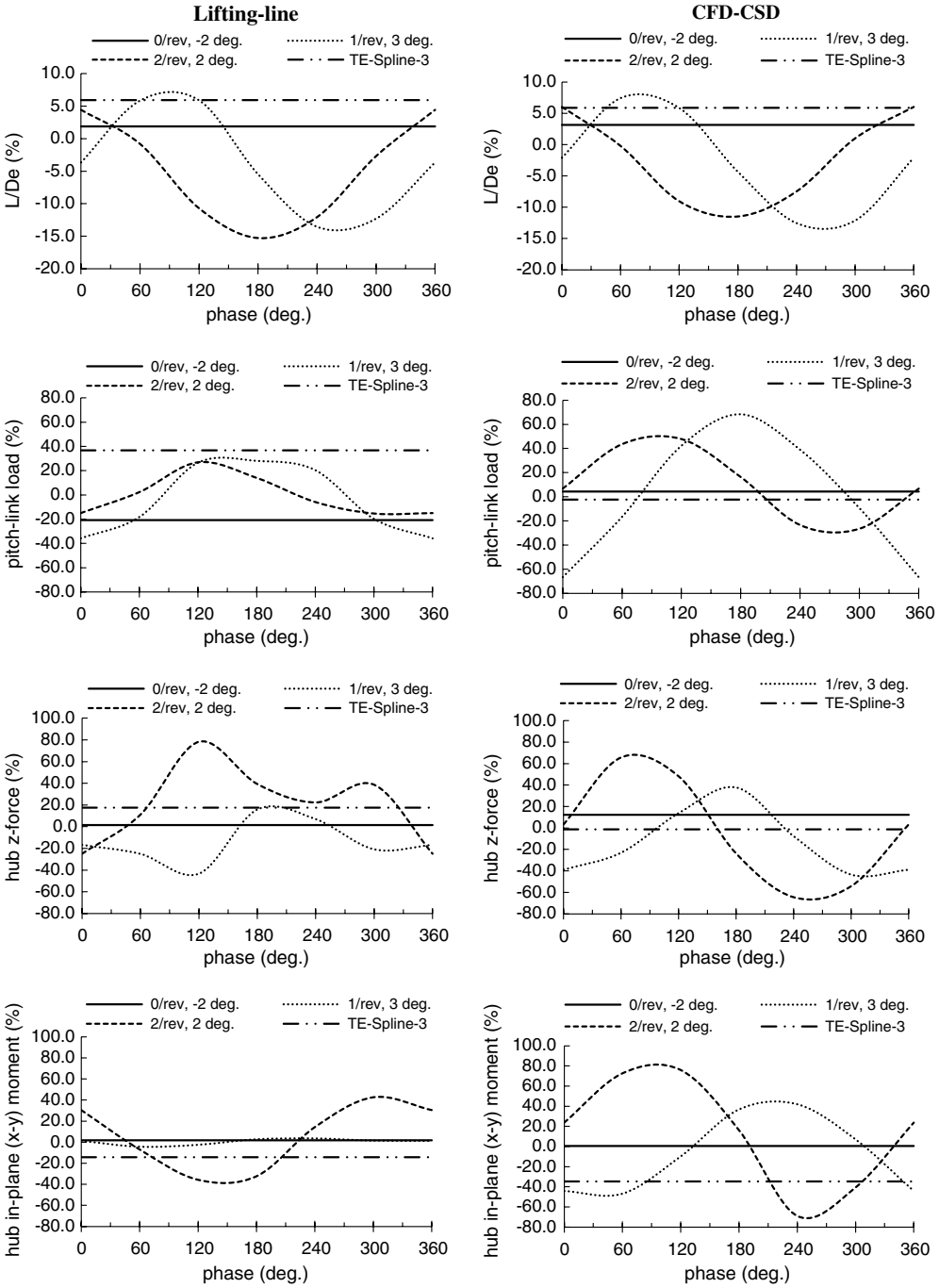

Fig. 2 Calculated performance and structural loads with TED (15%R × 10%C wide) applied between 67.5 to 82.5% R with N/rev deployment, where $N = 0$, 1, and 2, and nonharmonic deployment using lifting-line and CFD–CSD calculations. The flight condition is high-speed forward flight (c8534). Peak-to-peak loads are plotted for pitch-link load, flap- and lag-bending moments, and 4/rev vibratory loads are plotted for hub force and moment.

of the dynamic morphing of the blade. The airfoil surface is represented by NURBS [18] curves, which are defined by a set of control points. The number of control points and their positions were chosen to match the baseline airfoil geometries. Then the TED and LED motions are defined in terms of the displacements at control points [17]. The morphed TED and LED geometries are shown in Fig. 1. In this study the shape of TED was slightly modified from [17] to closely resemble a trailing-edge flap. This was done to precisely define the width of the flap chord. The TED is characterized by the inner and outer radial locations, $R^{\text{TED}}_{\text{inner}}$ and $R^{\text{TED}}_{\text{outer}}$, respectively, the deflection angle, δ_{TED}, and the chord wise width, C_{TED}. The LED also has similar parameters as shown in the same figure. The active-twist was simulated by applying a moment couple of equal and opposite strength at 20 and 90% radii, which results in near-linear distribution of twist over the span of the rotor blade. It is assumed that the active-twist concept does not involve sectional airfoil shape change.

Rotor Geometry and Flight Conditions

The baseline rotor studied in this paper is the UH-60A rotor. The rotor properties are listed in Table 1. Two key steady-level forward flight conditions of the NASA/Army UH-60A Airloads Program [19] are examined: (1) high-speed (c8534) and (2) high-thrust (c9017), steady-level forward flights. The flight conditions are listed in Table 2. The high-speed flight is characterized by transonic flow on the advancing side which causes high-vibratory hub loads. The high-

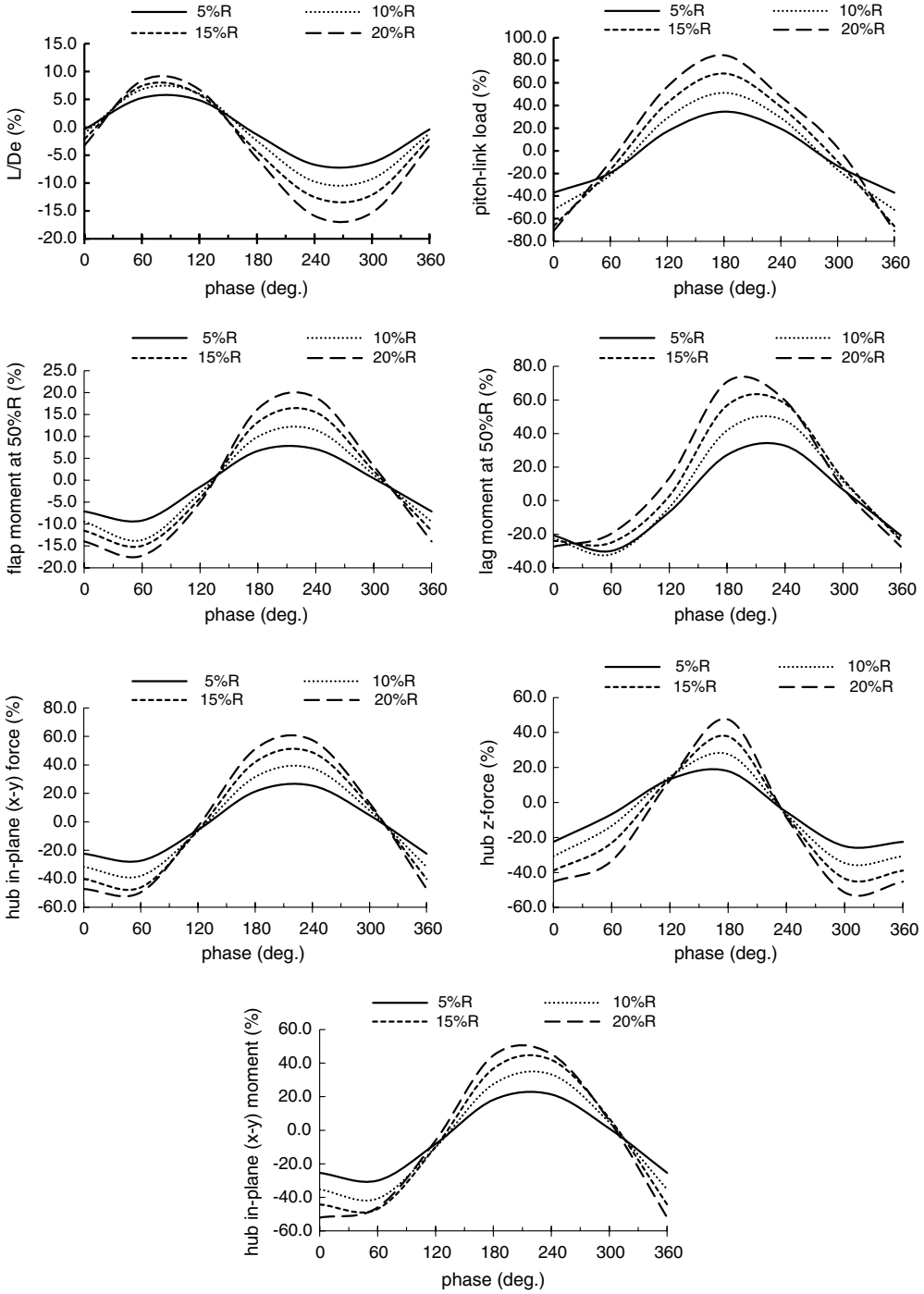

Fig. 3 Calculated performance and structural loads for TED ($X\%R \times 10\%C$ wide) radial span variation for 6 deg amplitude, 1/rev deployment (CFD–CSD calculations), 5% R is 72.5–77.5% R, 10% R is 70–80% R, 15% R is 67.5–82.5% R, and 20% R is 65–85% R. The flight condition is high-speed forward flight (c8534). Peak-to-peak loads are plotted for pitch-link, flap-, and lag-bending moments, and 4/rev vibratory loads are plotted for hub force and moment.

thrust flight is characterized by dynamic stall on the retreating blade side. The previous study ([17]) showed that the TED and active-twist deployment appear suitable for high-speed forward flight whereas the LED appears suitable for high-thrust forward flight. The current parametric study examined only those flight conditions.

Simulation Methods

For CFD simulations, WIND-US-HELI [20,21] is used, and for CSD, RCAS [22] is used. WIND-US-HELI uses unstructured, overlapping grids, which lends large flexibility in grid generation (including the possibility of automated grid generation using tetrahedral, hexahedral, prismatic, and pyramidal cell types). It includes a second order temporal scheme with Newton updates and dual-time-stepping for convergence acceleration.

The WIND-US-HELI and RCAS are coupled using the standard "delta-formulation" technique [23–25]. The coupling of WIND-US-HELI and RCAS was validated for the c8534 and c9017 flight conditions in [17]. The UH-60A rotor structure was modeled using nonlinear beam elements and also included modeling of other components such as swash-plate, push-rod and pitch-horn. The current RCAS structural model for the UH-60A rotor blade has been previously validated in [26]. The WIND-US-HELI code has been further enhanced to model the morphing rotor geometries [17].

The trim state of the rotor is specified in terms of the following trim targets: rotor thrust, hub pitch and roll moments, and propulsive force. This particular way of trimming is referred to as propulsive trim. The fuselage drag (propulsive force) is estimated using an equivalent flat-plate area, f, of 35.14 ft^2 (or $f/A=$ 0.01553, where A is the rotor disk area). This model has been shown

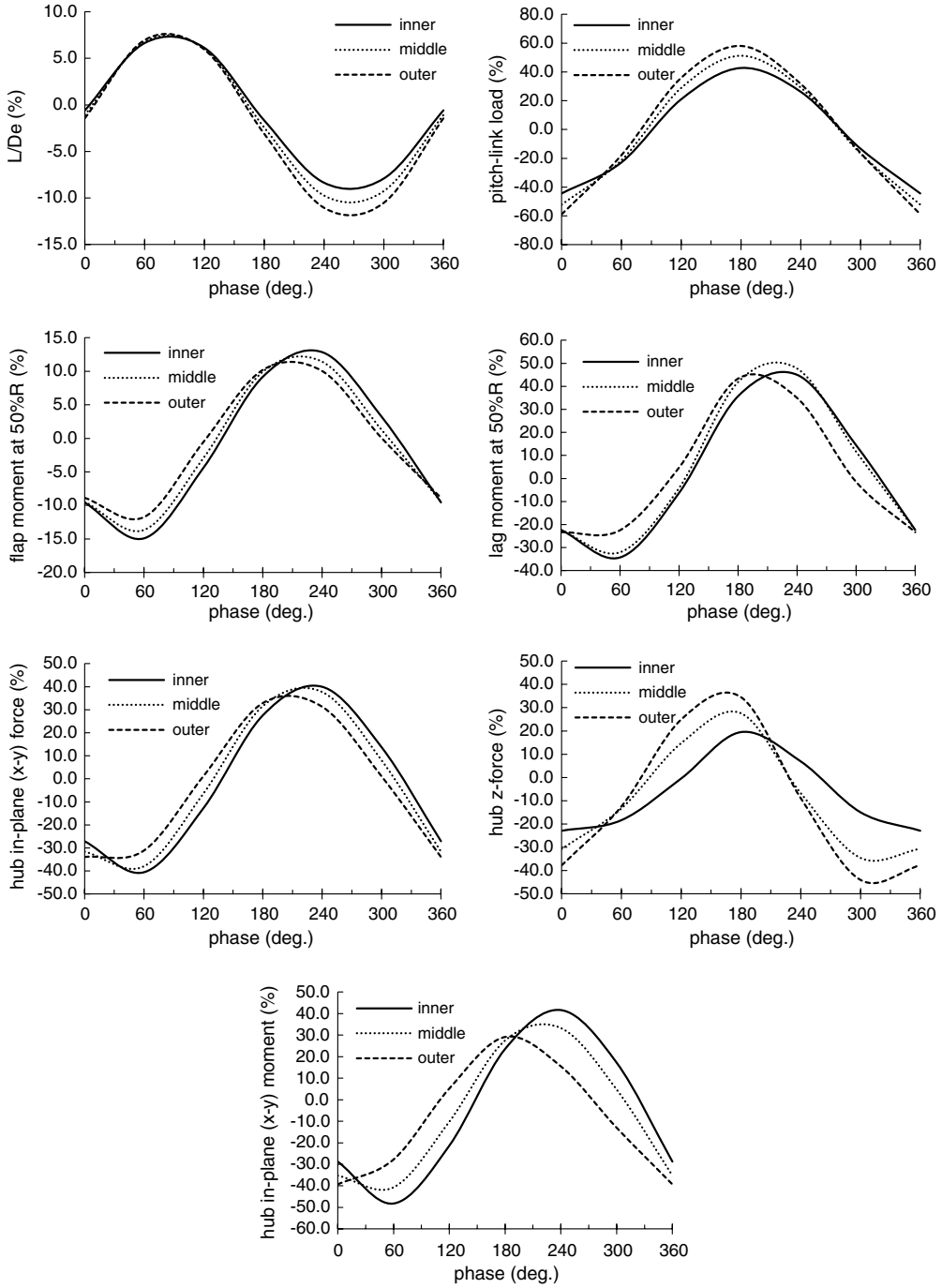

Fig. 4 Calculated performance and structural loads for TED (10%R × 10%C wide) radial location variation for 6 deg amplitude, 1/rev deployment (CFD–CSD calculations), inner is 65–75% R, middle is 70–80% R, and outer is 75–85% R. The flight condition is high-speed forward flight (c8534). Peak-to-peak loads are plotted for pitch-link load, flap- and lag-bending moments, and 4/rev vibratory loads are plotted for hub force and moment.

to give good performance correlations [27]. To achieve the trim targets listed in Table 2, collective, lateral-cyclic, longitudinal-cyclic, and (hub) shaft forward tilt angle are used as trim variables. The trim variables computed (CFD–CSD coupled analysis) that satisfy the trim targets for the c8534 and c9017 flight conditions are listed in Table 3.

For the high-speed forward flight, the computed power coefficient was found to be within 2% of the measured value. For the high-thrust forward flight, however, the power correlation significantly deteriorates compared with the high-speed condition. The calculated power was found to be quite sensitive to the prescribed thrust (trim target) which significantly affected the extent of stall on the retreating side. The computational model (numerical setup, turbulence model, and CFD-mesh) used for the validation of the baseline (no active control) rotor validation was, for predictive consistency, held to be the same for all the simulations presented here.

The structural properties of the blade (mass, moment of inertia, bending- and torsional-stiffness, etc.) would strongly depend on the structural properties of the actuator machinery, details of the blade cavity housing the actuator, and particulars of the actuator-blade assembly. Also, these would be significantly different for TED, LED, and active-twist. In this work, therefore, the structural properties of the baseline (no active control) rotor are used, without any modifications, for the analyses of the active control concepts. An assessment from a pure aeromechanical perspective of the rotor loads due to various dynamic blade shapes for improving the rotor aerodynamic efficiency is carried out, relative to the baseline rotor. If the structural properties are modified due to active control machinery,

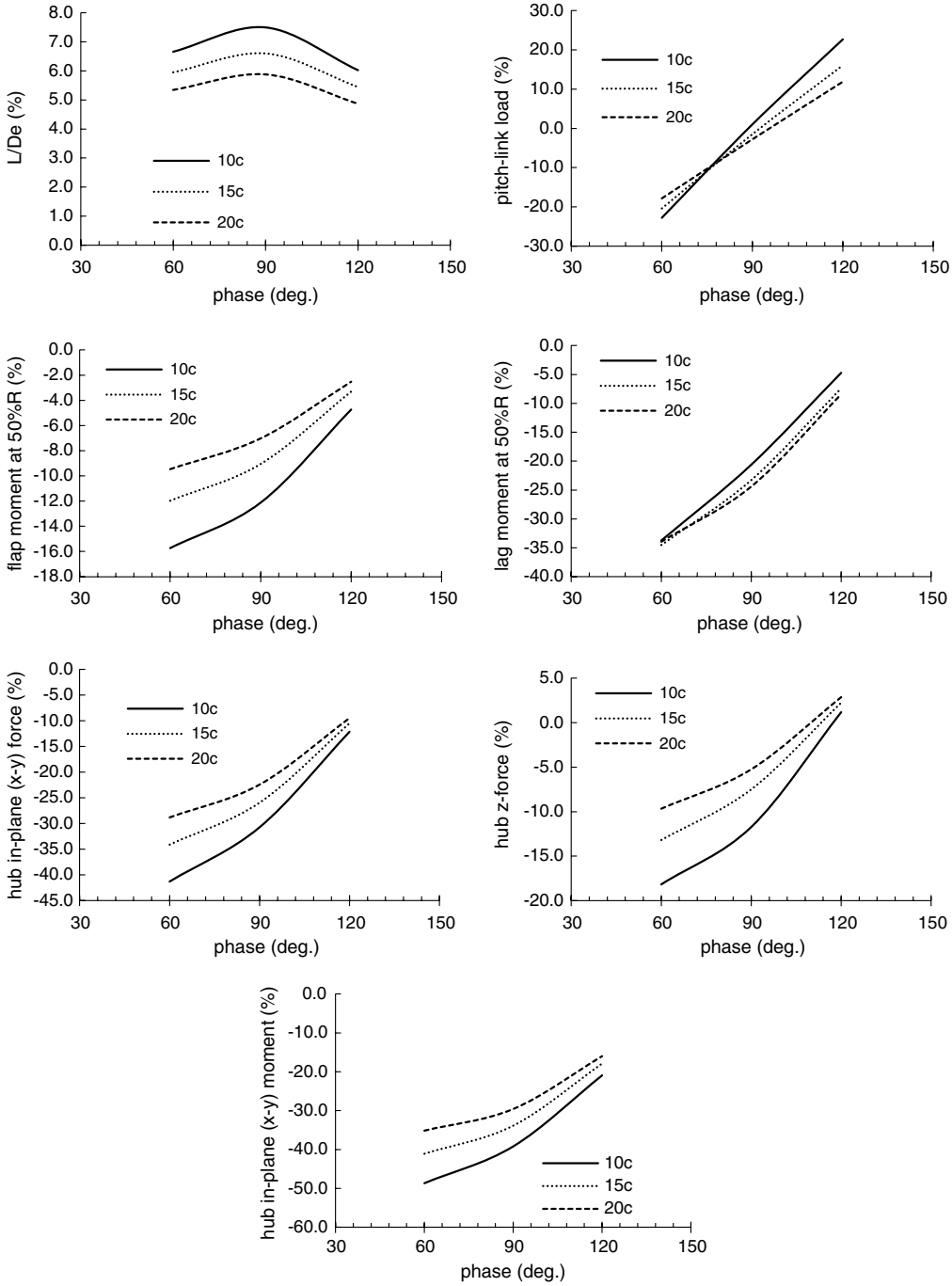

Fig. 5 Calculated performance and structural loads for TED (10% *R* wide) chord width variation for 1/rev deployment (CFD–CSD calculations). The TED amplitudes for 10, 15, and 20% *C* chord widths are 6, 4, and 3 deg, respectively, in order to maintain a constant vertical displacement of the trailing-edge. The flight condition is high-speed forward flight (c8534). Peak-to-peak loads are plotted for pitch-link load, flap- and lag-bending moments, and 4/rev vibratory loads are plotted for hub force and moment.

then optimal deployment schedules for performance improvement and the rotor loads might change. However, the performance gains and the associated reduction in rotor loads, which results from the counteraction of the fundamental flow features by the active control devices, are expected to remain the same.

Metrics

For forward flight at moderate to high-advance ratios ($\mu > 0.1$) the aerodynamic efficiency of the rotor is well represented by the ratio of lift to effective drag, L/D_e [28], given by

$$\frac{L}{D_e} = \frac{L}{\frac{P}{V} - F_p}$$

where, L is rotor lift which perpendicular to the wind direction, D_e is effective drag, P is rotor power, V is forward speed, and F_p is propulsive force. Since all the calculations in this work are performed using the propulsive trim strategy, F_p is a constant for a given flight condition. Then a change in L/D_e is also an indirect measure of the change in rotor power: an increase in L/D_e implies a decrease in rotor power for desired lift [or, $L/D_e = k_1/(P - k_2)$, k_1 and k_2 are constants for a given flight condition]. The performance improvement (power saving) is estimated purely from an aeromechanical perspective and only for the main rotor. The power expended by the actuators/control system in order to produce the desired deformations has not been included as it is a function of the particular actuation technology employed and its efficiency.

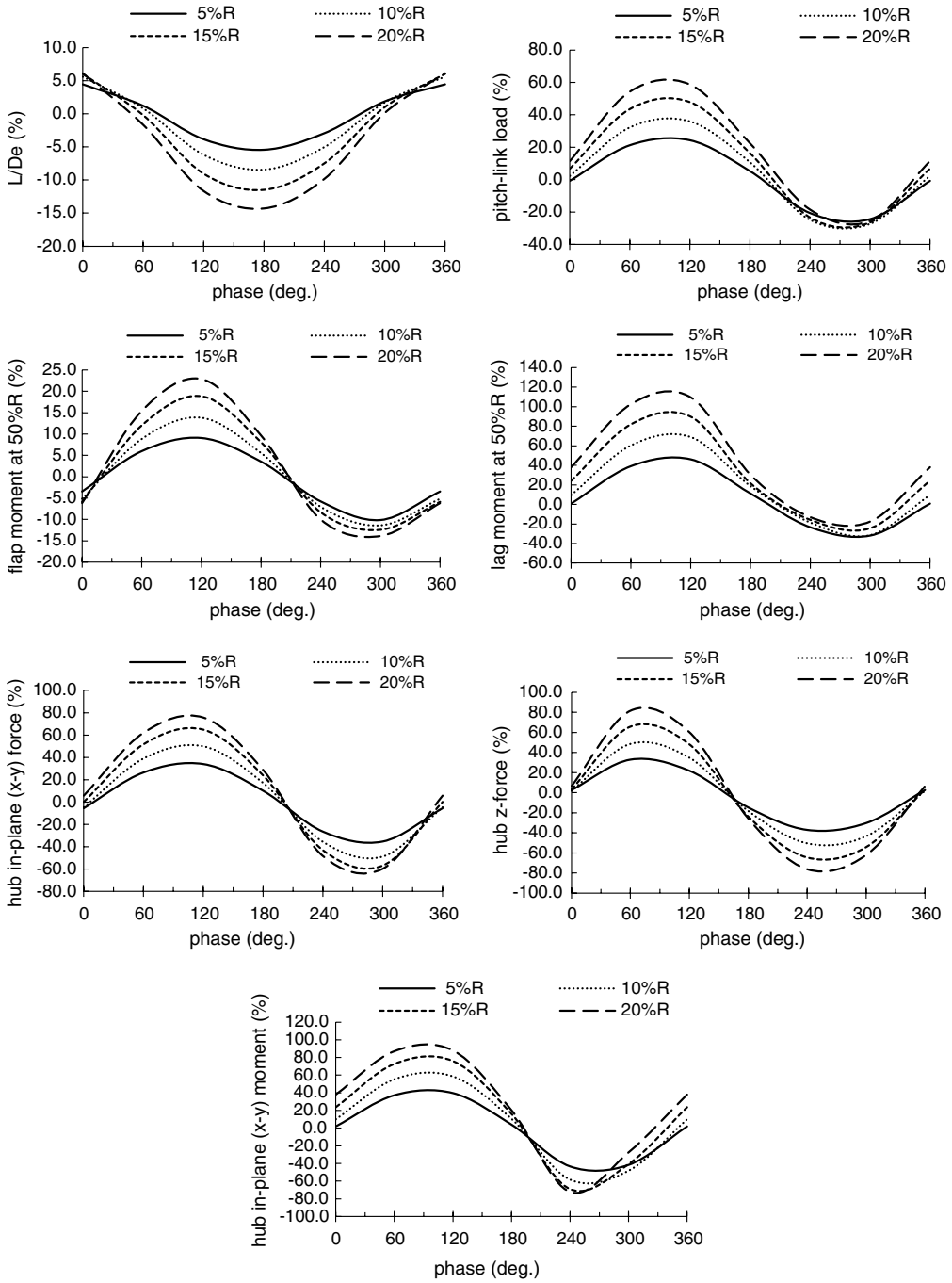

Fig. 6 Calculated performance and structural loads for TED ($X\%R \times 10\%C$ wide) radial-width variation for 4 deg amplitude, 2/rev deployment (CFD–CSD calculations), 5% R is 72.5–77.5% R, 10% R is 70–80% R, 15% R is 67.5–82.5% R, and 20% R is 65–85% R. The flight condition is high-speed forward flight (c8534). Peak-to-peak loads are plotted for pitch-link load, flap- and lag-bending moments, and 4/rev vibratory loads are plotted for hub forces and moments.

For structural loads, the metrics are: (1) peak-to-peak magnitude of the pitch-link load ($F_{p\text{-link}}$, which is also a measure of the total root torsional moment on the blade); (2) peak-to-peak magnitude of the blade flap bending (M_y) and lag-bending (M_z) moments at the 50% radial location; and (3) 4/rev hub (nonrotating) vibratory loads, which are: a) in-plane ($x-y$) hub force, $F_{xy,4/\text{rev}} = (F^2_{x,4/\text{rev}} + F^2_{y,4/\text{rev}})^{1/2}$; (b) vertical hub force, $F_{z,4/\text{rev}}$; and (c) in-plane hub moment, $M_{xy,4/\text{rev}} = (M^2_{x,4/\text{rev}} + M^2_{y,4/\text{rev}})^{1/2}$.

Baseline Performance and Loads with Trailing-Edge Deflection

The rotor performance and loads predicted using lifting-line comprehensive analysis and coupled CFD–CSD analysis are presented in Fig. 2. The TED configuration of 15% R radial span, from 67.5% R to 82.5% R, and 20% C chordwise width was used. Both harmonic and nonharmonic deployment schedules are considered for the high-speed flight condition (c8534). The harmonic deployment is of the form: $\delta_{\text{TED}} = A\cos(N\psi + \phi)$, where A is the amplitude, N is the frequency, and ϕ is the phase angle. The phase angle is varied from 0 to 360 deg in the steps of 60 deg. The frequency is varied to be 0/rev, 1/rev, and 2/rev. For each frequency, the amplitude was varied to be 1, 2, 3, 4, and 5 deg and the optimal value that resulted in best performance is presented here [17]. A nonharmonic schedule is also considered where a 2 deg upward deflection on the advancing side and a 5 deg downward deflection on the retreating side are applied. This schedule is referred to as *TE-SPLINE-3* in [17]. The performance and structural loads predicted using CFD–CSD and lifting-line comprehensive analysis are pre-

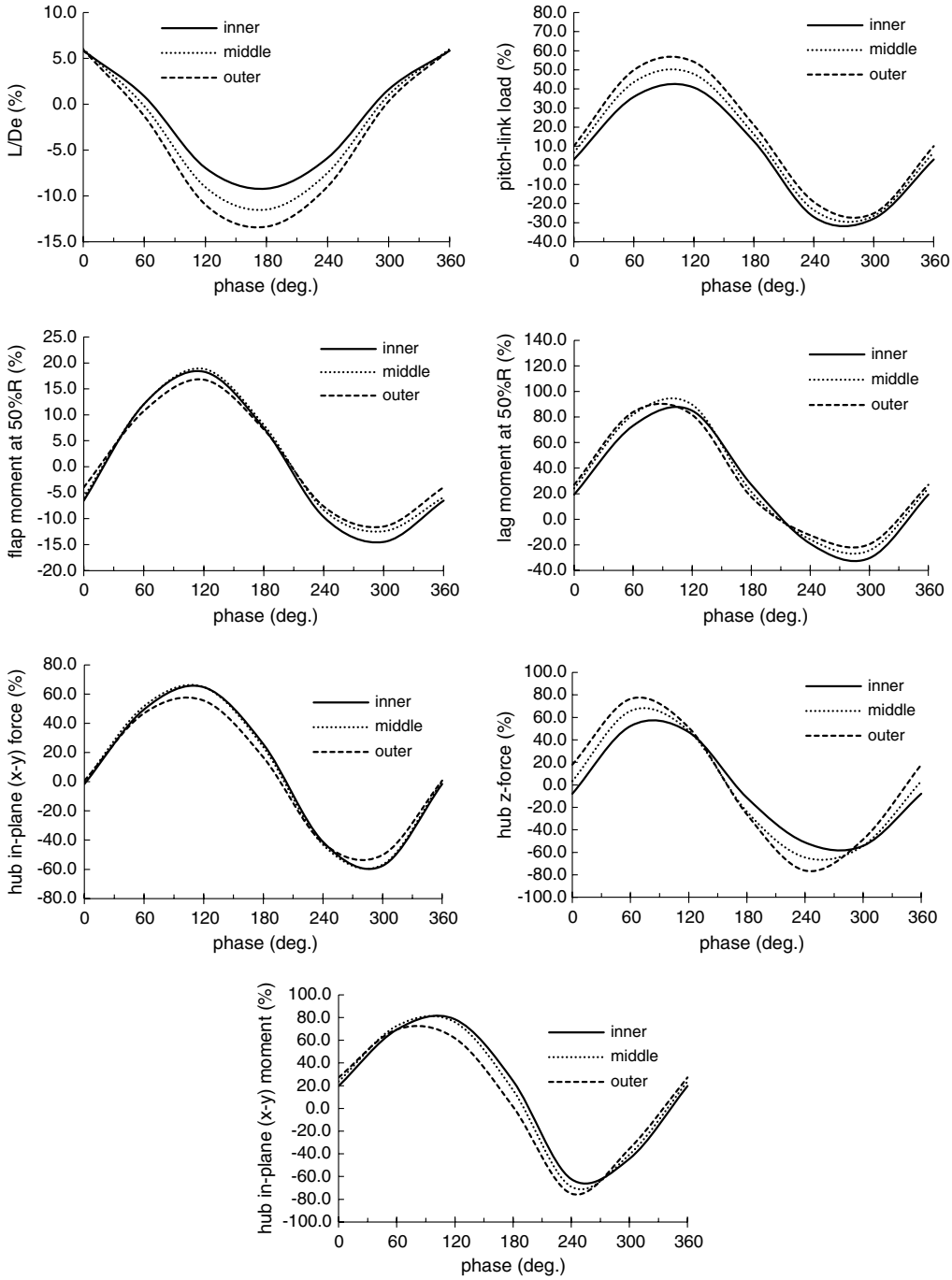

Fig. 7 Calculated performance and structural loads for TED (15%R × 10%C wide) radial location variation for 4 deg amplitude, 2/rev deployment (CFD–CSD calculations), inner is 62.5–77.5% R, middle is 67.5–82.5% R, and outer is 72.5–87.5% R. The flight condition is high-speed forward flight (c8534). Peak-to-peak loads are plotted for pitch-link load, flap- and lag-bending moments, and 4/rev vibratory loads are plotted for hub force and moment.

sented in Fig. 2. The performance prediction between the two analyses is quite consistent in both the trends and amplitude for harmonic and for the nonharmonic, TE-SPLINE-3, schedules. The predictions for hub vibratory loads, on the other hand, are significantly different. (The same holds true for flap- and lag- moment predictions which are not shown in the figure for brevity.) These discrepancies can be attributed to the fact that the lifting-line analysis characteristically suffers from predicting three-dimensional, unsteady, transonic pitching moment on the blade outboard stations on the advancing side which also causes significant phase errors in the prediction of the normal (lift) forces [29]. These comparisons highlight the need for employing high-fidelity computations using CFD for studies involving structural loads analysis. All the subsequent studies are carried out using CFD–CSD coupled analysis.

Trailing-Edge Deflection at High Speed (c8534)

In this section a parametric study on the TED deployment schedule and sizing is presented with the objective of maximizing the performance improvement while reducing all the structural loads.

In [17] a generic, smooth shape was used for TED which did not resemble a trailing-edge flap whereas in the present study the shape was modified to closely resemble a trailing-edge flap (see Fig. 1) in order to precisely prescribe the chord width. The TED shape used in [17] most closely resembles the new TED shape with 10% *C* flap width. The parametric study is carried out based on variation of this baseline TED configuration.

First, the radial span variation of TED is carried out for a fixed middle radial location of 75% *R* and a chord width of 10% *C*. The best performing span is down-selected. For the selected span, its

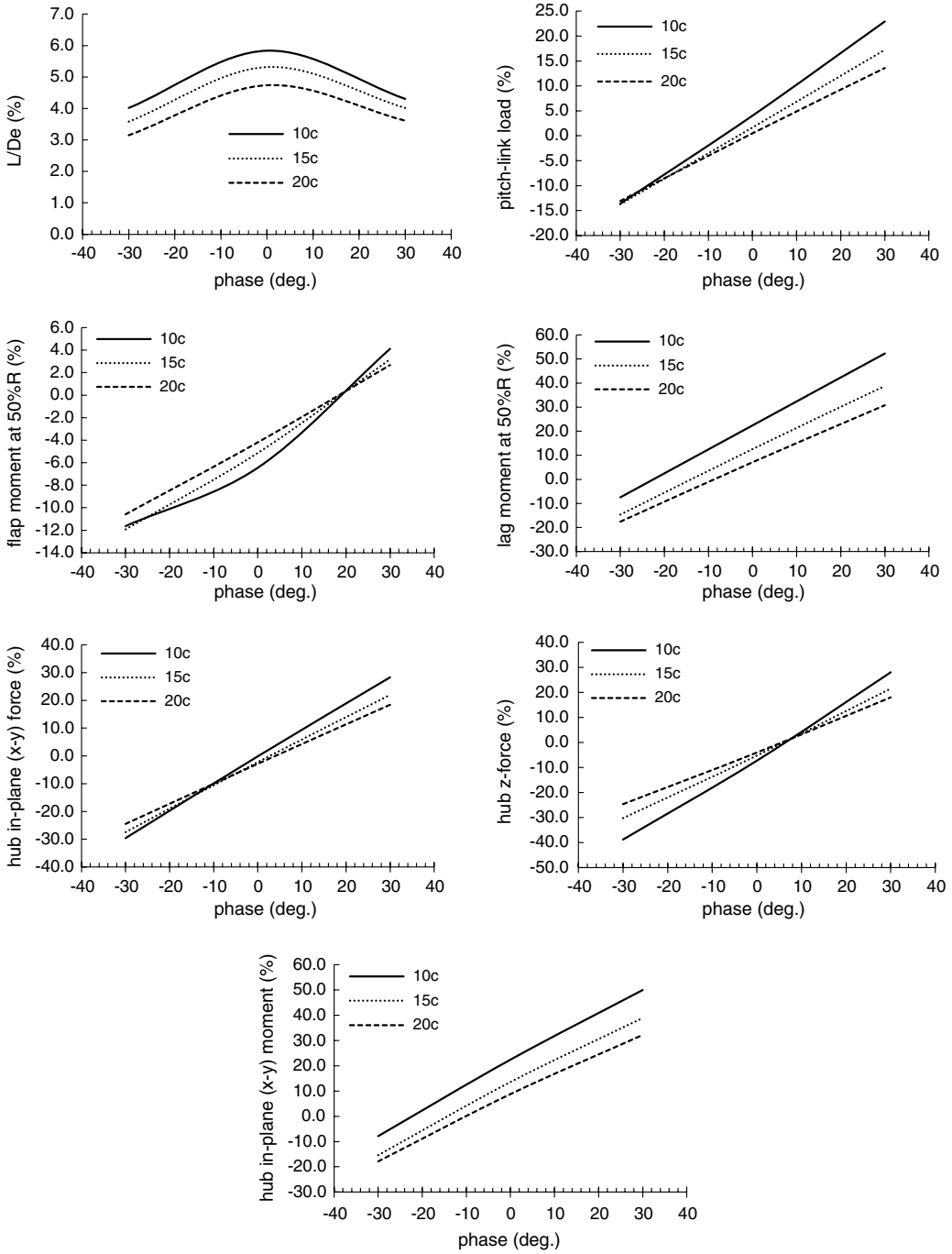

Fig. 8 Calculated performance and structural loads for TED (15% *R* wide) chord width variation for 2/rev deployment (CFD–CSD calculations). The TED amplitudes for 10, 15, and 20% *C* chord widths are 4, 2.67, and 2 deg, respectively, in order to maintain a constant vertical displacement of the trailing-edge. The flight condition is high-speed forward flight (c8534). Peak-to-peak loads are plotted for pitch-link load, flap- and lag-bending moments, and 4/rev vibratory loads are plotted for hub force and moment.

Table 4 TED sizing study of the TE-SPLINE-3 nonharmonic schedule

Case	$R_{\text{inner}}, \%R$	$R_{\text{outer}}, \%R$	$R_{\text{mean}}, \%R$	Radial width, $R_{\text{outer}} - R_{\text{inner}}$	Chord width, $\%C$
A	72.5	77.5	75	5	10
B	70	80	75	10	10
C	67.5	82.5	75	15	10
D	65	85	75	20	10
E	70	90	80	20	10
F	60	80	70	20	10
G	60	80	70	20	15
H	60	80	70	20	20

middle radial location is varied while still keeping the chord width fixed to 10% C and best location is down-selected. Finally, for the selected span and its middle radial location, the chord width is varied and best chord width is selected. This parametric study is carried out for 1/rev, 2/rev and nonharmonic deployment schedules.

The following parametric variations are considered: 1) deployment schedule 1/rev, 2/rev, and nonharmonic; 2) flap radial span, $R^{\text{TED}}_{\text{outer}} - R^{\text{TED}}_{\text{inner}}$; 3) flap middle radial location, $(R^{\text{TED}}_{\text{outer}} + R^{\text{TED}}_{\text{inner}})/2$; and 4) flap chord width, C_{TED}.

Parametric Sweep of TED Geometric Sizing with 1/rev Deployment

The 1/rev deployment of TED is studied in this section. The 1/rev deployment does not interfere with the rotor trim state even though 1/rev inputs are also used for the primary control inputs since for a given 1/rev TED excitation, a propulsive trim procedure is carried out and a new set of trim control inputs are obtained that meet the trim targets.

Flap Radial Span Variation

Four variations of the radial spans are considered: 5% R, 10% R, 15%R, and 20% R. The flap middle radial location is held fixed at 75% R and the chordwise width is held fixed at 10% C. The

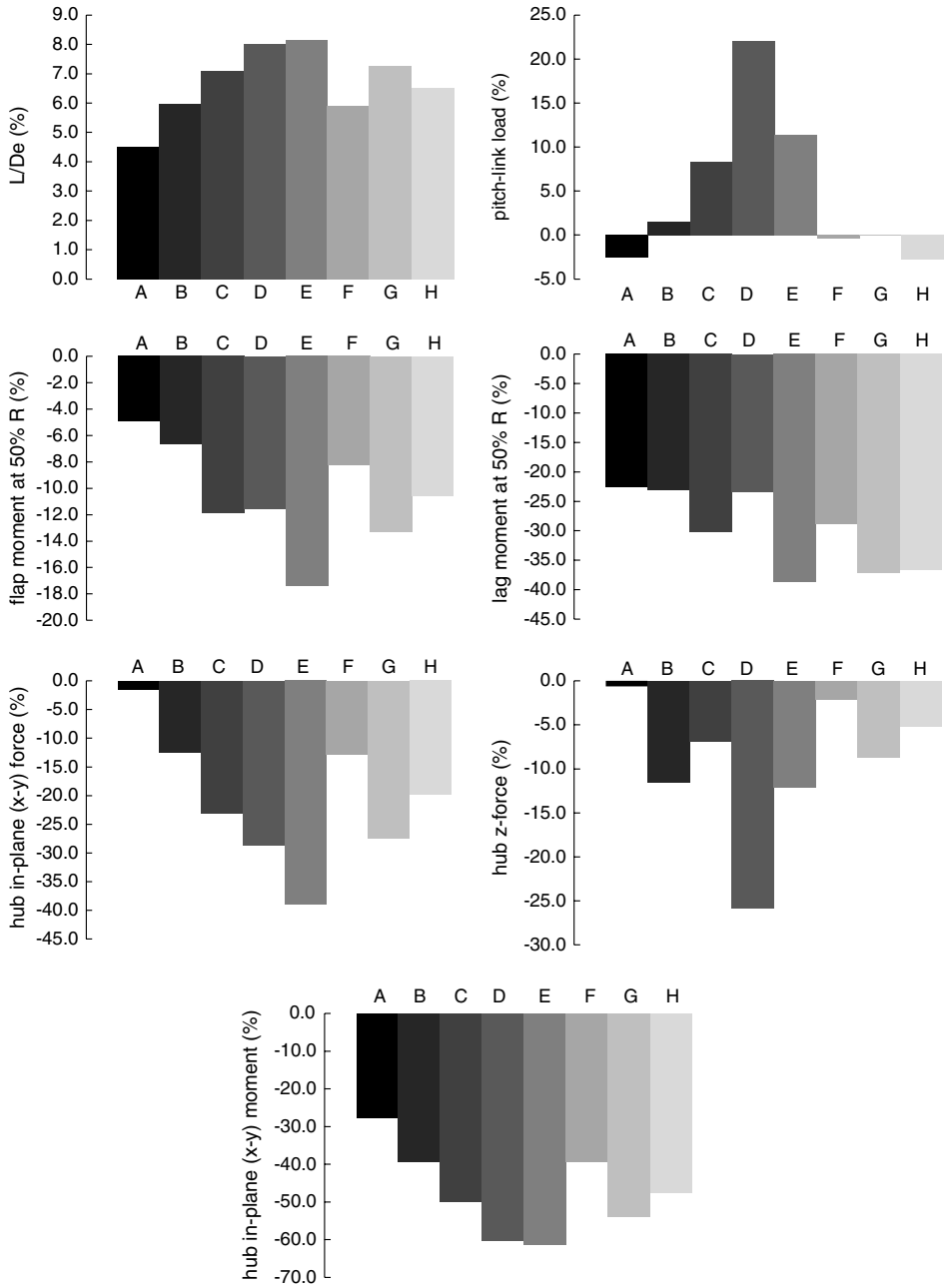

Fig. 9 Calculated performance and structural loads for TED radial width, radial location, and chord width variation for TE-SPLINE-3 deployment (CFD–CSD calculations). The flight condition is high-speed forward flight (c8534). Peak-to-peak loads are plotted for pitch-link load, flap-, and lag-bending moments, and 4/rev vibratory loads are plotted for hub force and moment.

amplitude of deployment is chosen to 6 deg. (In [17] a generic, smooth shape was used for TED and best performance was obtained using a 3 deg deflection. The new TED shape with 10% C and 6 deg deflection closely resembles this TED shape and is used to carry out the parametric studies.) The phase angle is varied from 0 to 360 deg in the steps of 60 deg. The maximum performance gain is seen at phase angle slightly below 90 deg. Figure 3 shows that the maximum gains in L/D_e with the 5, 10, 15, and 20% R spanwise widths are about 5.7, 7.5, 8.0, and 9.0%, respectively. However, at this phase angle, the pitch-link load and the hub vibratory z-force also moderately increase. As the phase angle is reduced below 90 deg, there is a small reduction in the performance gain and a relatively large reduction in the structural loads. Hence, with the reduced phase angle, the overall objective of improving the performance without penalizing the structural loads can be achieved. The 20% R span TED deployed at 60 deg phase angle results in about 8.4% performance gain and reduction in the structural loads: the pitch-link load reduces by about 10%, flap bending moment reduces by about 17%, and lag-bending moment reduces by about 20%. The hub vibratory in-plane force, vertical force, and in-plane moment decrease by about 49, 33, and 46%, respectively. On the other hand, with the 10% R span at 80 deg phase angle, the maximum gain in performance is about 7.5% whereas the pitch-link load and hub vibratory vertical force remain unchanged and other loads are reduced: flap bending moment reduces by about 12%, and lag-bending moment reduces by about 22%. The hub vibratory in-plane force and moment both decrease by about 30%. Compared with a wider 20% R span, the 10% R span TED only slightly compromises the performance and is attractive

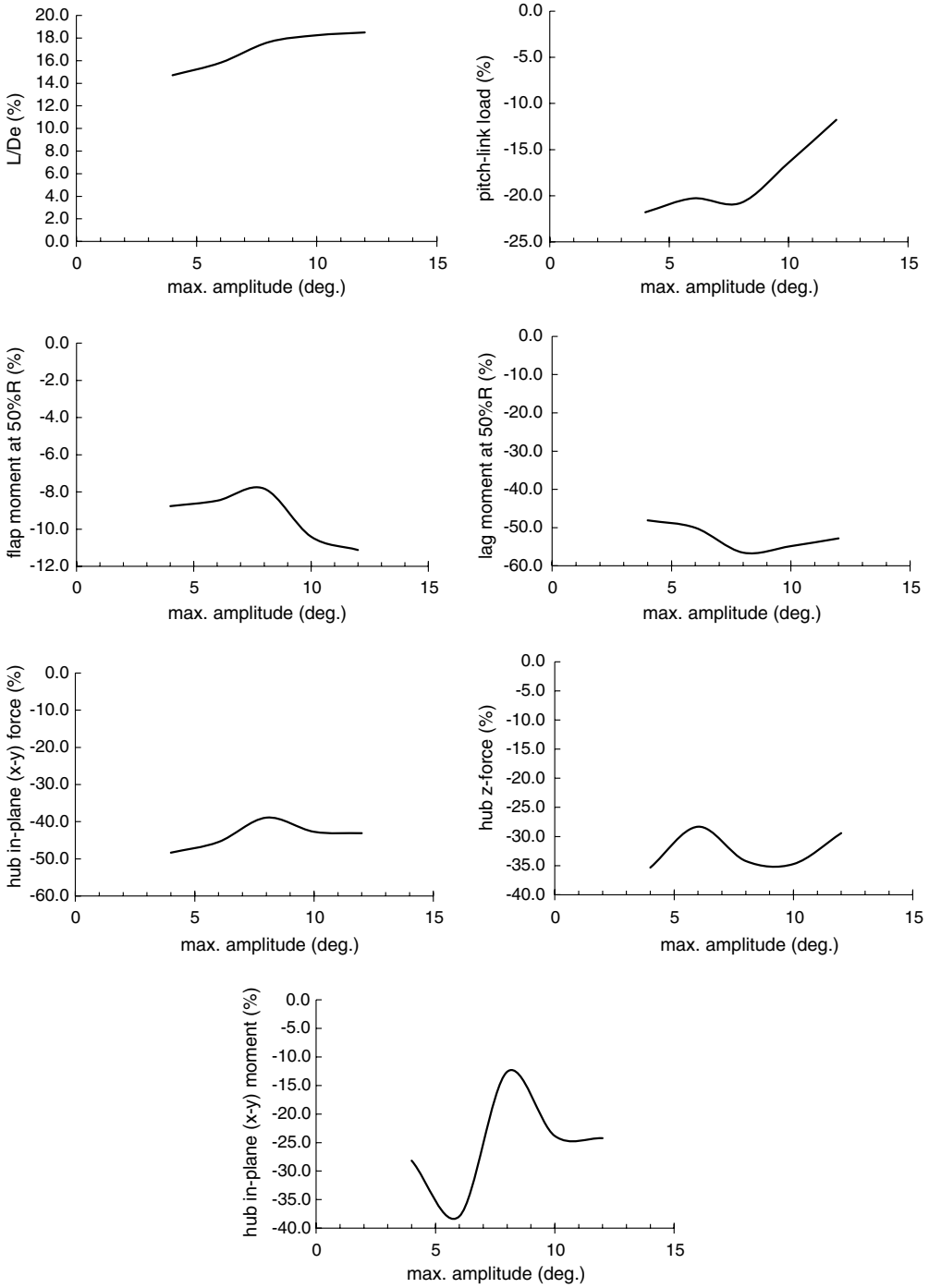

Fig. 10 Calculated performance and structural loads for LED (24%R × 10%C wide) deployed only on the retreating side: effect of variation of maximum deflection on the retreating side (CFD–CSD calculations). The flight condition is high-thrust forward flight (c9017). Peak-to-peak loads are plotted for pitch-link load, flap- and lag-bending moments, and 4/rev vibratory loads are plotted for hub force and moment.

from the actuator design perspective as it implies a smaller actuation system (less weight penalty) and less power to realize the TED. The 10% R span TED is, therefore, investigated further with the variation of the middle radial location.

Flap Middle Radial Location Variation

The 10% R span TED is further investigated for improvements in performance and loads with the variation of the flap middle radial location. The chordwise width is held fixed at 10% C and the amplitude of deployment is 6 deg. Three radial positions are considered: inner, extending from 65 to 75% R; middle, from 70 to 80% R; and, outer, from 75 to 85% R.

The performance and loads are shown in Fig. 4. The peak of the performance is unaffected by the radial location variation. Based on the trends presented in the figure, the best case seems to be the 10% R TED at the inner location and deployed at the phase angle of 85 deg, which is the point where the performance is maximum. The performance gain is about 7.3% which is only slightly reduced compared with the middle location where it is 7.5%. The pitch-link load reduces by about 5%, flap bending moment reduces by about 13%, and lag-bending moment reduces by about 24%. The hub vibratory in-plane force, vertical force, and in-plane moment decrease by about 32, 12, and 41%, respectively.

The 10% R TED at the inner location is further investigated with the variation of the flap chord width.

Flap Chord Width Variation

Next, the effect of trailing-edge flap chord width is studied. Three chord widths, 10, 15, and 20% C, are studied for the 10% R span TED and at the inner radial location of 70% R. The performance and loads are shown in Fig. 5. As pointed out above, for 1/rev deployment, L/D_e is maximum near the phase of 90 deg so the chord width studies were carried out only in its vicinity at the phase angles of 60, 90, and 120 deg. For the 10% C case, the amplitude of deflection is 6 deg. whereas for 15 and 20% chord, amplitude is decreased to maintain the same vertical displacement of the trailing-edge point so amplitudes are 4 and 3 deg., respectively. The 10% C TED has a higher performance gain over the 15 and 20% C widths.

As noted in the previous section, the optimum phase angle is around 85 deg. where the L/D_e gain is 7.3%. The pitch-link load reduces by about 5%, flap bending moment reduces by about 13%, and lag-bending moment reduces by about 24%. The hub vibratory in-plane force, vertical force, and in-plane moment decrease by about 32, 12, and 41%, respectively.

Parametric Sweep of TED Geometric Sizing with 2/rev Deployment

The results for the geometric sizing variation with the 2/rev deployment are presented in the following sections.

Flap Radial Span Variation

As in the previous section, four radial spans are studied: 5, 10, 15, and 20% R. All are centered at 75% R and the chordwise width is 10% C. The effect on performance and loads are shown in Fig. 6. The amplitude of deployment is 4 deg. (In [17] a generic, smooth shape was used for TED and best performance was obtained using a 2 deg deflection. The new TED shape with 10% C and 4 deg deflection closely resembles this TED shape and is used to carry out the parametric studies.) The peak performance gain is seen at the phase angle of 0 deg. With 5% R span TED, the gain is about 4.4% and, on the other hand, with 20% R span TED, it is about 6.1%. At this phase angle, however, there is a penalty in structural loads. Since the structural loads decrease as the phase angle is decreased below 360 deg, a phase angle between 330 and 360 deg is preferred in order to keep the loads low. An optimal configuration appears to be the 15% R span TED with the phase angle of 345 deg, where the L/D_e gain is compromised from 6.0 to about 5.0% and structural loads penalty is reduced. The pitch-link load remains about the same, flap bending moment reduces by about 6%, and lag-bending moment increases by about 18%. The hub vibratory in-plane force, and vertical force decrease by about 18 and 10%, respectively, while the in-plane moment increases by about 10%. The penalty in lag-bending moment and hub in-plane moment can be avoided at the cost of reduced performance gain of around 4%.

Flap Middle Radial Location Variation

The 15% R span TED is studied further for improvements in performance and loads with the variation of the flap middle radial location. Three radial positions are studied: inner from 62.5 to 77.5% R; middle from 67.5 to 82.5% R; and outer from 72.5 to 87.5% R, where the middle radial locations are 70, 75 and 80% R, respectively. The chordwise width is 10% C and amplitude of deployment is 4 deg, as in the previous section. The performance and loads are shown in

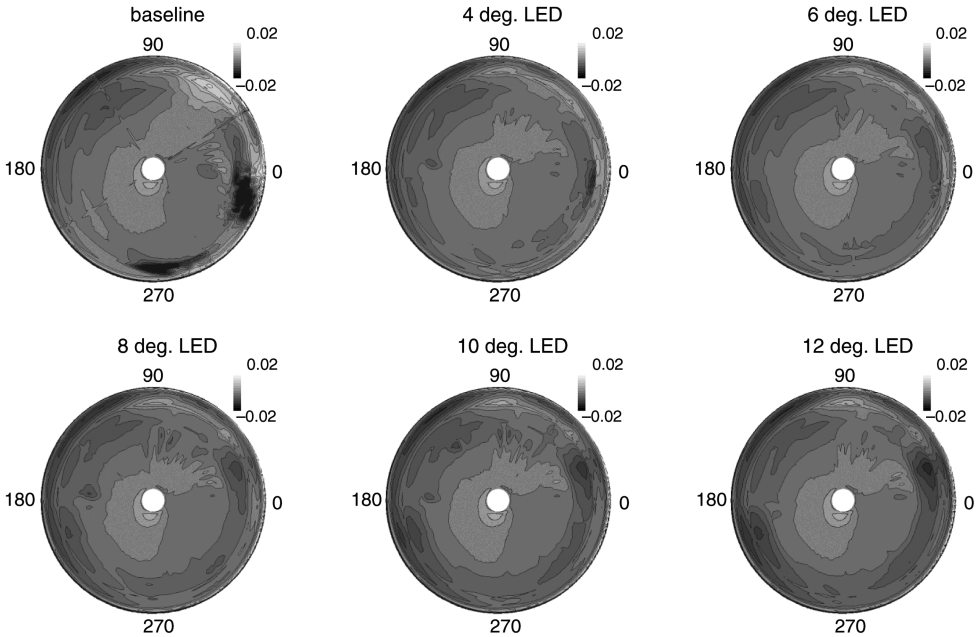

Fig. 11 Blade sectional pitching moment (M^2C_M) for LED (24%R × 10%C wide) deployed only on the retreating side: effect of variation of maximum deflection angle, $\theta_{\mathrm{LE,max}}$, on the retreating side (CFD–CSD calculations). The black spots on the retreating side of the baseline case signify dynamic stall events. The dynamic stall is largely subsided with a 6 deg LED deployment. The flight condition is high-thrust forward flight (c9017).

Fig. 7. The structural loads are reduced when the inner configuration is used. With the inner configuration, at the phase angle of 340 deg, the performance gain is about 4.7%, the pitch-link load reduces by about 7%, flap bending moment reduces by about 9%, and lag-bending moment remains unchanged. The hub vibratory in-plane force and vertical force decrease by about 20 and 30%, respectively, while the in-plane moment remains unchanged. The 15% *R* TED at the inner middle radial location is studied further with the flap chord width variation.

Flap Chord Width Variation

In this section, the effect of trailing-edge chord width is studied. Three chord widths, 10, 15, and 20% *C*, are studied for the 15% *R* span TED and the inner radial location of 70% *R*. The performance and loads are shown in Fig. 8. The parametric studies of the radial widths and locations presented above show that the peak performance occurs near the phase angle of 0 deg. Therefore, chord width variations are carried out only in the vicinity of 0 deg at the phase angles of −30 (330), 0 (360), and 30 deg. For the 10% *C* case the deployment amplitude is 4 deg. For the 15 and 20% *C*, it is decreased to 2.67 and 2 deg, respectively, in order to maintain the same vertical displacement of the trailing-edge point. The 10% *C* configuration at the phase angle of around 0 deg shows the most performance improvement. However, rotor loads increase at the same time. The optimum configuration appears to be the 10% *C* configuration at the phase angle of around 340 deg which achieves the performance improvement and loads reduction at the same time.

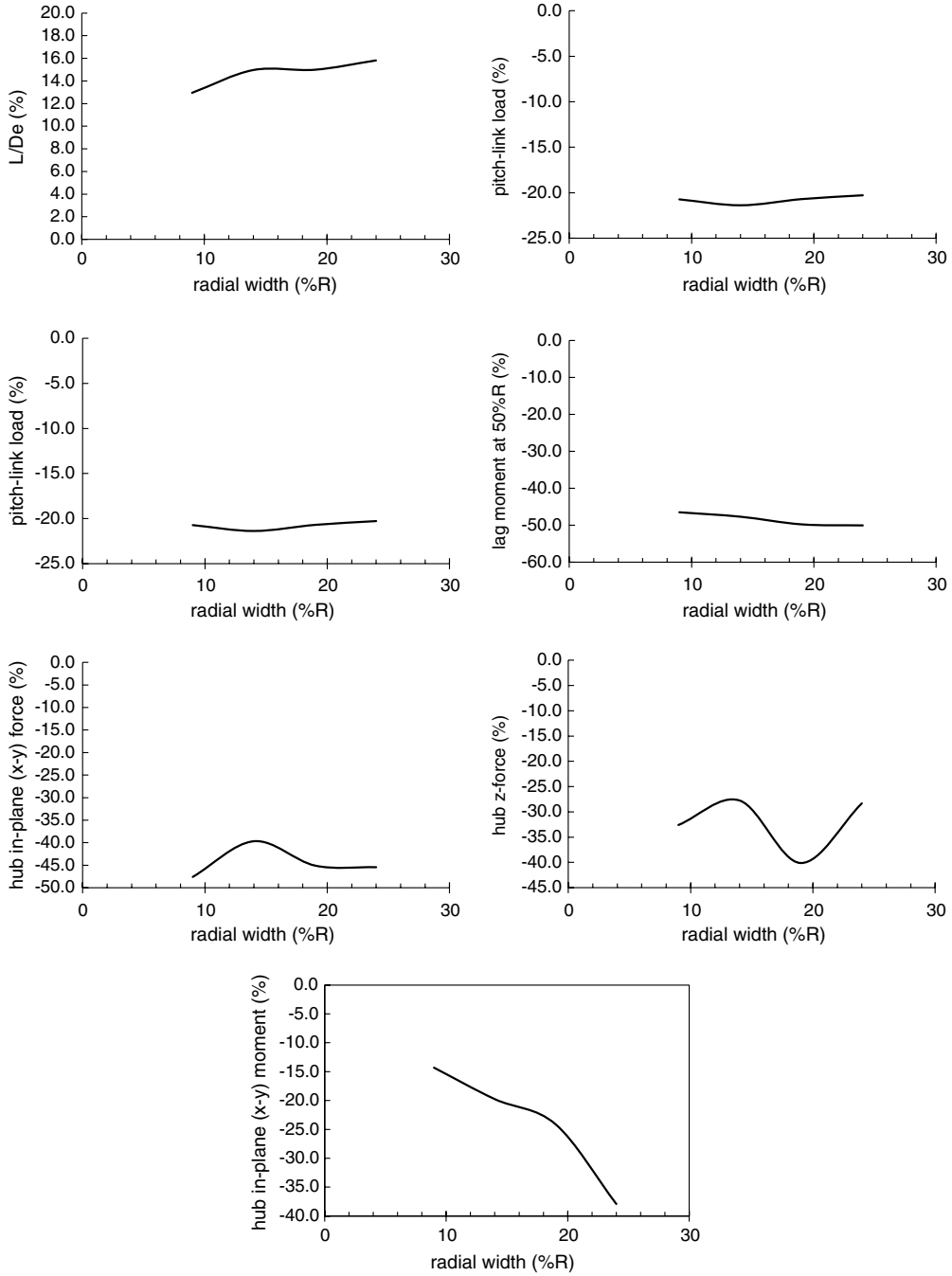

Fig. 12 Calculated performance and structural loads for LED (10% *C* chord width) deployed only on the retreating side: effect of variation of radial width (CFD–CSD calculations). The deflection on the retreating side is 6 deg. The outer radial location is fixed at 91.5% radial. The inner radial location is varied to be 82.5, 77.5, 72.5, and 67.5% radius. The flight condition is high-thrust forward flight (c9017). Peak-to-peak loads are plotted for pitch-link load, flap- and lag-bending moments, and 4/rev vibratory loads are plotted for hub force and moment.

As noted above, the L/D_e gain is about 4.7% and all the structural loads are about the same or reduced. The pitch-link load reduces by about 7%, flap bending moment reduces by about 9%, and lag-bending moment remains unchanged. The hub vibratory in-plane force and vertical force decrease by about 20 and 30%, respectively, while the in-plane moment remains unchanged.

Parametric Sweep of TED Geometric Sizing with Nonharmonic Deployment

A nonharmonic deployment scheme, where on the advancing side an upward deflection of 2 deg is applied and on the retreating side a downward deflection of 5 deg is applied, was previously studied in [17] and therein referred to as *TE-Spline-3*. In that study, the TED was applied from 67.5 to 82.5% *R* and the chord width of 20% *C* was used. In [17] a generic, smooth shape was used for TED. The new TED shape with 10% *C* chord width closely resembles this TED shape with 4 deg upward deflection on the advancing side and 10 deg downward deflection on the retreating side. Under the present study, a parametric study is carried out where the TED radial span, radial location, and the chord width are varied. Table 4 summarizes the parametric variations. The effect on performance and loads is shown in Fig. 9. As shown in the figure, the radial span variation of 5, 10, 15, and 20% *R* showed that the best performance is seen with the 20% *R*. However, the pitch-link load also increases as the TED radial span is increased. The middle radial location variation of the 20% *R* span TED is carried out next for three configurations: inner, middle, and outer radial locations with the middle location of 70, 75 *R*, and 80% R, respectively. With the inner configuration there is no penalty

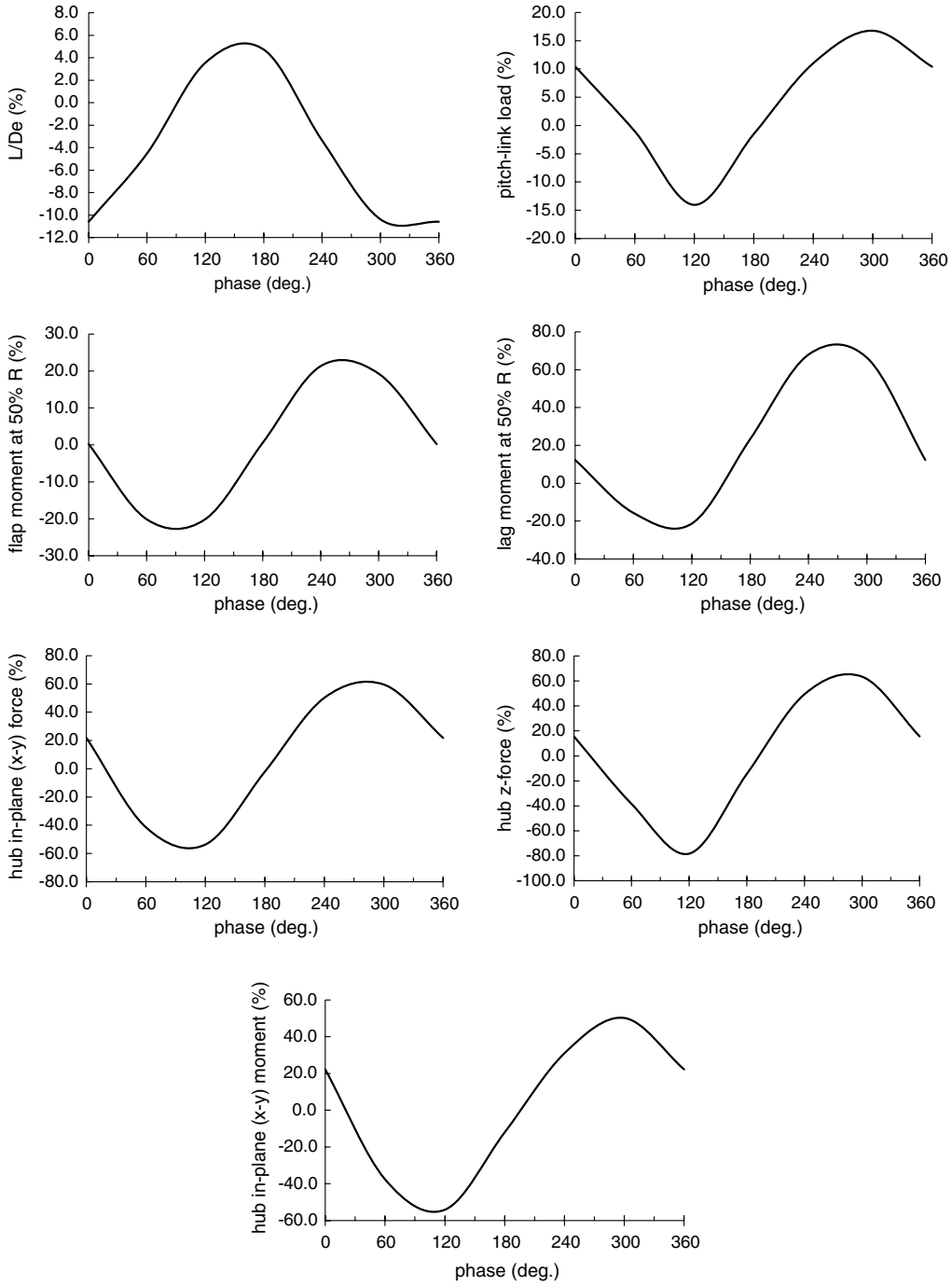

Fig. 13 Calculated performance and structural loads using CFD for 2/rev. and 2 deg amplitude active-twist deployment (CFD–CSD calculations). The flight condition is high-speed forward flight (c8534). Peak-to-peak loads are plotted for pitch-link load, flap- and lag-bending moments, and 4/rev vibratory loads are plotted for hub force and moment.

in the pitch-link load. The inner location is therefore studied further for flap chord width variation. Three chord flap widths: 10, 15, and 20% *C* are studied for the 20% *R* span TED at 70% *R* (inner) middle radial location. As before, for 15 and 20% *C* the amplitudes on the advancing side and retreating sides were reduced to maintain the same vertical displacement of the trailing edge. The chordwise variation shows that the 15% *C* results in the largest performance gain, the pitch-link loads remain unchanged, and all other structural loads are reduced. This configuration achieves about 7.3% performance gain. The flap bending moment reduces by about 13%, and lag-bending moment reduces by about 37%. The hub vibratory in-plane force, vertical force, and in-plane moment decrease by about 27, 9, and 54%, respectively.

Leading-Edge Deflection at High Thrust (c9017)

The baseline LED configuration studied in [17], radial span of LED was 24% *R* and chord width was 10% *C*. The best performance was obtained with deployment of 10 deg downward droop only on the retreating side where the performance gain was 18.2%. In the following sections, further parametric studies are carried on the amplitude of LED on retreating side and the LED radial span. The objective is to maximize the LED for performance and structural loads for the high-thrust, high-altitude, forward flight (c9017). First, a parametric sweep is carried out on the retreating side amplitude of the LED deployment and then for the down-selected amplitude, a parametric sweep of the radial span is carried out.

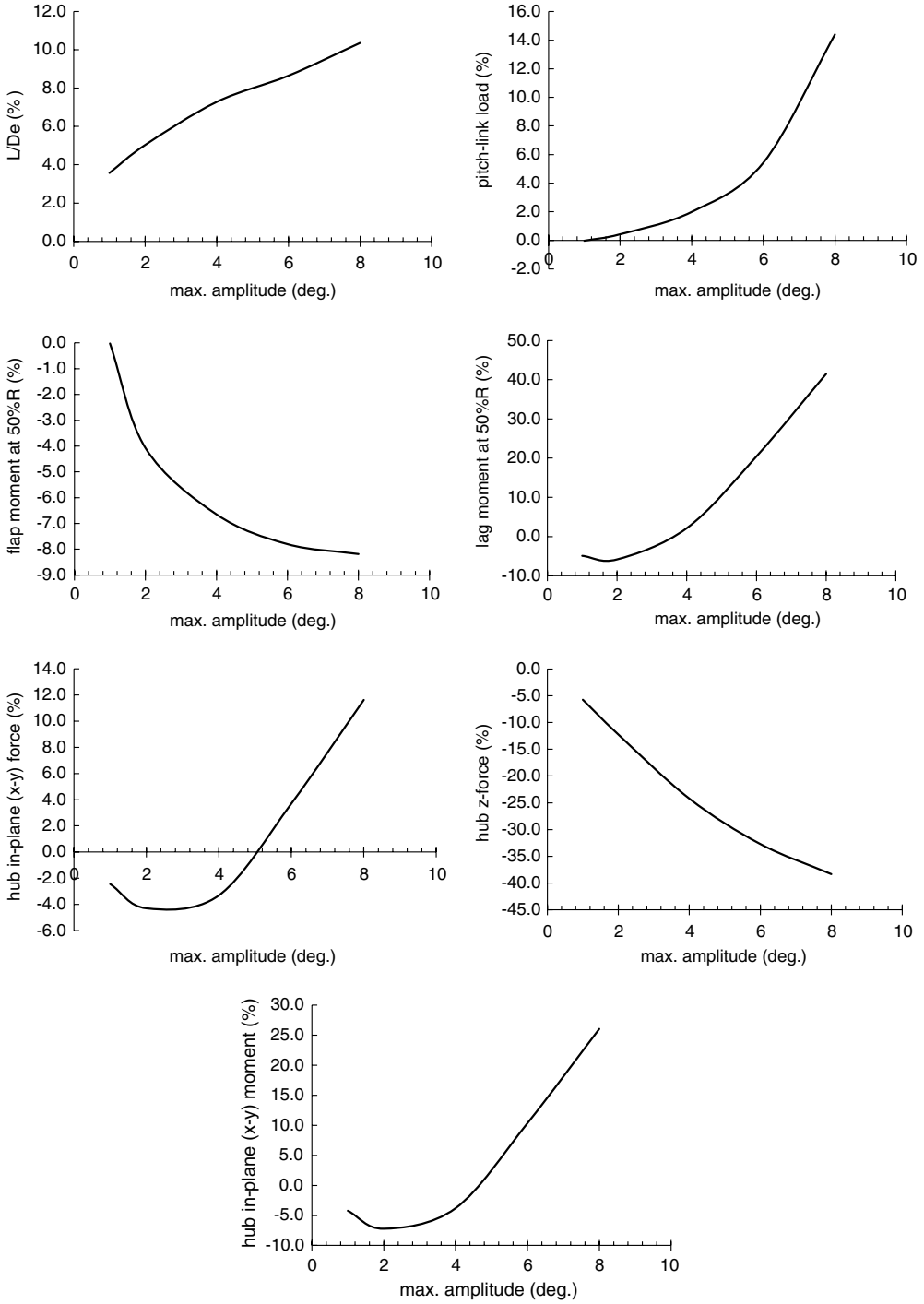

Fig. 14 Calculated performance and structural loads for active-twist (moment couple at 20 and 90% *R*) deployed only on the advancing side: effect of variation of maximum deflection on the advancing side (CFD–CSD calculations). The flight condition is high-speed forward flight (c8534). Peak-to-peak loads are plotted for pitch-link load, flap-, and lag-bending moments, and 4/rev vibratory loads are plotted for hub force and moment.

Table 5 Performance gains and rotor loads reduction for high-speed flight (C8534) with the studied morphing concepts

Morphing	Deployment schedule	Performance improvement	$F_{p\text{-link}}$	M_y	M_z	*Hub vibratory loads*		
						$F_{xy,4/\text{rev}}$	$F_{z,4/\text{rev}}$	$M_{xy,4/\text{rev}}$
Trailing-edge deflection	1/rev, span 10% R, middle span 70% R, chord width 10% C	7.3%	−5%	−13%	−24%	−32%	−12%	−41%
Trailing-edge deflection	2/rev, span 15%, middle span 70% R, chord width 10% C	4.7%	−7%	−9%	0%	−20%	−30%	0%
Trailing-edge deflection	Nonharmonic (TE-SPLINE-3), span 20% R, middle span 70% R, chord width 15% C	7.3%	0%	−13%	−37%	−27%	−9%	−54%
Active-twist	Deployment on the advancing-side-only of 4 deg pitch-up	7.3%	+2%	−6%	0%	−4%	−22%	−5%

Table 6 Performance gains and rotor loads reduction for high-speed flight (C9017) with the studied morphing concepts

Morphing	Deployment schedule	Performance improvement	$F_{p\text{-link}}$	M_y	M_z	*Hub vibratory loads*		
						$F_{xy,4/\text{rev}}$	$F_{z,4/\text{rev}}$	$M_{xy,4/\text{rev}}$
Leading-edge deflection	Deployment on the advancing-side-only of 6 deg downward	15.0%	−21%	−7%	−48%	−39%	−28%	−20%

Parametric Sweep of LED Retreating Side Amplitude with Retreating-Side-Only Deployment

For the case of retreating-side-only schedule, a parametric sweep is carried on the magnitude of the downward deflection, $\theta_{\text{LED,max}}$, on the retreating side, where it is varied to be 4, 6, 8, 10, and 12 deg. The radial extent is from 67.5 to 91.5% R and the chord width is 10% C. The effect on the performance and loads is shown in Fig. 10. There is a major increase in L/D_e of 18.5% at a LED amplitude of 12 deg. With the 10 deg amplitude, the increase in L/D_e remains practically unchanged at 18.3%, and when the amplitude is reduced to 4 deg: there is only a small decrease in performance from 18.5 to a 14.8% increase. A 6 deg deflection seems preferable which results in the performance increase of about 15.8% and, also, at the same time reduces the pitch-link load by about 20% and the hub vibratory in-plane moment by about 37%. The flap bending moment reduces by about 8% and lag-bending moment reduces by about 50%. The hub vibratory in-plane force and vertical force decrease by about 45 and 27%, respectively. The sectional pitching moment (M^2C_m) variation over the rotor disk is shown in Fig. 11. The dynamic stall events appear as dark blue regions on the disk around the phase angles of 180 and 330 deg. Even with a relatively small 6 deg downward droop on the retreating side, the two stall regions are largely reduced. A higher that 6 deg downward droop marginally increases the performance and can be used if the additional actuation power requirement is not high.

Parametric Sweep of LED Radial Span with Retreating-Side-Only Deployment

A study of variation of the radial span is carried out to assess the possibility of reducing the radial span of LED. In these calculations the downward deflection is applied only on the retreating side and amplitude of deflection is 6 deg, which is down-selected in the previous section. Since the dynamic stall occurs on the outboard regions, the radial span variation studies are conducted keeping the outer location fixed at 91.5% R and varying the inner location to be 67.5, 72.5, 77.5, and 82.5% R so that the radial span varies from 24 to 9% R, respectively. The loads and performance variation are shown in Fig. 12. As the radial span is decreased from 24 to 9% the L/D_e reduces from about 15.8 to about 12.9%. The best configuration seems to be about 14% R where the performance gain is about 15.0%. All the structural loads considered are significantly reduced: the pitch-link load reduces by about 21%, flap bending moment reduces by about 7%, and lag-bending moment reduces by about 48%. The hub vibratory in-plane force, vertical force, and in-plane moment decrease by about 39, 28, and 20%, respectively.

In summary, the 14% R wide LED of 6 deg amplitude appears to be an overall the best choice considering performance, structural loads, and the actuator sizing.

Active-Twist at High Speed (c8534)

In this section, the effect of active-twist on performance and loads for the high-speed forward flight condition (c8534) are presented for 2/rev harmonic and advancing-side-only deployments.

The parametric study of harmonic deployment schedules presented in [17] showed that the best gain in performance were obtained with 2/rev deployment with 2 deg amplitude and 150 deg phase angle. The gain in L/D_e is about 5.0%. In principle, the active-twist concept is similar to the individual blade control. The individual blade control with 2/rev input was studied in a wind tunnel on a full-scale BO-105 rotor in [9] and similar trends were reported for the hub vibratory loads as the present active-twist results in Fig. 13: a reduction in hub loads was seen near 90 deg phase angle whereas the maximum increase in hub loads was seen near 240 deg. A non-harmonic schedule of active-twist was also considered where it was applied only the advancing side. With a 4 deg twist on the advancing side the gain in L/D_e is about 7.3%. In the following section, a parametric sweep of the advancing side amplitude is carried out to maximize performance and reduce the structural loads at the same time.

A parametric sweep is carried out where the amplitude of twist on the advancing side is varied to be 1, 2, 4, 6, and 10 deg. The effect on performance and loads is shown in Fig. 14. The rotor L/D_e varies linearly with the amplitude but the loads vary nonlinearly. At amplitudes of 5 deg and higher even though there is good performance gains the structural loads increase significantly. Amplitude of around 4 deg seems optimal as it achieves a performance gain is about 7.3% and there is a minimal penalty in the structural loads. The pitch-link load increases by about 2%, flap bending moment reduces by about 6%, and lag-bending moment remain unchanged. The hub vibratory in-plane force, vertical force, and in-plane moment decrease by about 4, 22, and 5%, respectively.

Conclusions

Three morphing concepts (TED, LED, and active-twist) are investigated for the rotor aerodynamic performance improvements and their effects on the structural loads. A coupled framework employing a CFD module and a CSD module has been developed that allows for modeling of a morphing rotor. The CFD–CSD method is then used to assess the potential of various active rotor concepts in

improving the rotor aeromechanics. The baseline rotor considered is a full-scale UH-60A Blackhawk main rotor. Two key flight conditions of high-speed and high-thrust forward flights are studied. Parametric sweep of the deployment schedule and geometric sizing of the active control surface was carried and a down-selection is made based on the gains in performance and reduction in loads. The following conclusions are obtained:

1) The TED and active-twist deployment appear suitable for high-speed forward flight whereas the LED appears suitable for high-thrust forward flight. When deployed optimally, the performance of the rotor is improved and the structural loads are either reduced or unchanged for all the three concepts.

2) Trailing-edge deflection at high-speed forward flight case: A parametric study was carried on flap span, middle radial location, and chord width. With 1/rev deployment, the best configuration found is 10% R span TED with 70% R middle radial location, and 10% C chord width. It achieves about 7.3% gain in L/D_e and about a 3.3% reduction in rotor power, and up to 41% reduction in the hub vibratory load. With 2/rev deployment, the best configuration found is 15% R span TED also at 70% R middle radial location and 10% C chord width. It achieves a 4.7% gain in L/D_e and about a 2.3% reduction in power, and up to 30% reduction in hub vibratory loads. The nonharmonic deployment (advancing side 2.67 deg and retreating side 6.67 deg) of 20% R span, 70% R middle radial location, and 15% C chord width results in L/D_e gain of around 7.3% and about a 3.3% reduction in power, and up to 54% decrease in hub vibratory loads. The nonharmonic deployment appears most suitable among the three deployment schedule considering both the performance gain and reduction in the structural loads. These results are summarized in Table 5.

Leading-edge deflection at high-thrust forward flight case: the leading-edge deployment only on the retreating side results in best performance. A parametric study was carried on the magnitude of the retreating side amplitude as well as on the radial span. The 14% R span LED of 6 deg amplitude is the best choice considering performance, structural loads, and actuator sizing. The gain in performance is about 15.0% (reduction in power of 12.4%) and up to 40% reduction in hub vibratory loads. These results are summarized in Table 6.

Active-twist at high-speed forward flight case: the active-twist deployment only on the advancing side results in best performance. A parametric study was conducted where the amplitude of the advancing side was varied. The optimal amplitude appears to be around 4 deg. The performance gain is about 7.3% (reduction in power is about 3.3%) and there is up to 22% reduction in hub vibratory loads. These results are summarized in Table 5.

The parametric study presented here showed that significant improvements in the rotor performance, and at the same time reduction in rotor structural peak-to-peak and vibratory loads, can be achieved using a proper deployment schedule and geometric sizing of the active control surface.

In this study, the rotor performance improvement is presented purely from the aeromechanical perspective without adding the details or effect of the actuation machinery into the structural dynamics modeling or the power required to operate the machinery. The installation of actuator device on the blade would likely result in significant changes in the blade structural properties. However, since the performance improvements presented here are fundamentally due to the counteraction of three-dimensional unsteady transonic pitching moments at the high-speed flight condition, and due to dynamic stall at high-thrust flight condition, the aeromechanical improvements presented herein should hold with improved fidelity of structural modeling with modified blade properties and modeling of inertial effects. Only the optimal deployment schedule and geometric sizing might likely change.

Acknowledgments

This work is sponsored by U.S. Army Research, Development, and Engineering Command under SBIR Contract No. W911W6-08-C-0061. Technical monitors were Hyeonsoo Yeo and Mark Fulton at the U.S. Army Aeroflightdynamics Directorate.

References

[1] Chopra, I., "Status of Application of Smart Structures Technology to Rotorcraft Systems," *Journal of the American Helicopter Society*, Vol. 45, No. 4, Oct. 2000, pp. 228–252. doi:10.4050/JAHS.45.228

[2] Yeo, H., "Assessment of Active Controls for Rotor Performance Enhancement," *Journal of the American Helicopter Society*, Vol. 53, No. 2, April 2008, pp. 152–163. doi:10.4050/JAHS.53.152

[3] Cheng, R. P., and Celi, R., "Optimum Two-Per-Revolution Inputs for Improved Rotor Performance," *Journal of Aircraft*, Vol. 42, No. 6, Nov.–Dec. 2005, pp. 1409–1417. doi:10.2514/1.20884

[4] Kang, H., Saberi, H., and Gandhi, F., "Dynamic Blade Shape for Improved Helicopter Rotor Performance," *American Helicopter Society 65th Annual Forum Proceedings*, Grapevine, TX, 27–29 May 2009.

[5] Léon, O., Hayden, E., and Gandhi, F., "Rotorcraft Operating Envelope Expansion Using Extendable Chord Sections," *American Helicopter Society 65th Annual Forum Proceedings*, Grapevine, TX, 27–29 May 2009.

[6] Martin, P. B., McAlister, K. W., and Chandrasekhara, M. S., "Dynamics Stall Measurements and Computations for a VR-12 Airfoil with a Variable Droop Leading Edge," *American Helicopter Society 59th Annual Forum Proceedings*, Phoenix, AZ, 6–8 May 2003.

[7] Kerho, M., "Adaptive Airfoil Dynamic Stall Control," 43rd Aerospace Sciences Meeting and Exhibit, AIAA Paper 2005-1365, Reno, NV, 10–13 Jan. 2005.

[8] Mishra, A., Ananthan, S., and Baeder, J. D., "Coupled CFD/CSD Prediction of the Effects of Trailing Edge Flaps on Rotorcraft Dynamic Stall Alleviation," 47th AIAA Aerospace Sciences Meeting Including the New Horizons Forum and Aerospace Exposition, Orlando, FL, AIAA Paper No. 2009-891, 5–8 Jan. 2009.

[9] Jacklin, S. A., Blaas, A., Teves, D., and Kube, R., "Reduction of Helicopter BVI Noise, Vibration, and Power Consumption Through Individual Blade Control," *American Helicopter Society 51st Annual Forum Proceedings*, Fort Worth, TX, 9–11 May 1995.

[10] Jacklin, S. A., Haber, A., Simone, G. d., Norman, T. R., Kitaplioglu, C., and Shinoda, P., "Full-Scale Wind Tunnel Test of an Individual Blade Control System for a UH-60 Helicopter," *American Helicopter Society 58th Annual Forum Proceedings*, Montréal, 11–13 June 2002.

[11] Norman, T. R., Theodore, C., Shinoda, P., Fuerst, D., Arnold, U. T. P., Makinen, S., Lorber, P., and O'Neill, J., "Full-Scale Wind Tunnel Test of a UH-60 Individual Blade Control System for Performance and Vibration, Loads, and Noise Control," *American Helicopter Society 65th Annual Forum Proceedings*, Grapevine, TX, 27–29 May 2009.

[12] Nitzsche, F., Feszty, D., Waechter, D., Bianchi, E., Voutsinas, S., Gennaretti, M., Coppotelli, G., and Ghiringhelli, G. L., "The SHARCS Project: Smart Hybrid Active Rotor Control System for Noise and Vibration Attenuation of Helicopter Rotor Blades," 31st European Rotorcraft Forum, Paper No. 52, Florence, Italy, 13–15 Sept. 2005.

[13] Straub, F. K., Anand, V. R., Birchette, T. S., and Lau, B. H., "Wind Tunnel Test of the SMART Active Flap Rotor," *American Helicopter Society 65th Annual Forum Proceedings*, Grapevine, TX, 27–29 May 2009.

[14] Fulton, M. V., "Aeromechanics of the Active Elevon Rotor," *American Helicopter Society 61st Annual Forum Proceedings*, Grapevine, TX, 1–3 June 2005.

[15] Shin, S., Cesnik, C. E. S., and Hall, S. R., "Design and Simulation of Integral Twist Control for Helicopter Vibration Reduction," *International Journal of Control, Automation, and Systems*, Vol. 5, No. 1, Feb. 2007, pp. 24–34.

[16] Wilbur, M. L., Yeager, W. T., Jr., and Sekula, M. K., "Further Examination of the Vibratory Loads Reduction Results from the NASA/Army/MIT Active Twist Rotor Test," *American Helicopter Society 58th Annual Forum Proceedings*, Montreal, 11–13 June 2002.

[17] Jain, R., Szema, K. Y., Munipalli, R., Yeo, H., and Chopra, I., "CFD–CSD Analysis of Active Control of Helicopter Rotor for Performance Improvement," *American Helicopter Society 65th Annual Forum Proceedings*, Grapevine, TX, 27–29 May 2009.

[18] Piegl, L., and Tiller, W., *The NURBS Book*, 2nd ed., Springer–Verlag, New York, 1995.

[19] Kufeld, R. M., Balough, D. L., Cross, J. L., Studebaker, K. F., Jennison, C. D., and Bousman, W. G., "Flight Testing of the UH60A Airloads

Aircraft," *American Helicopter Society 50th Annual Forum Proceedings*, Washington, D.C., May 1994.

[20] Jain, R. K., Ramakrishnan, S. V., and Chen, C. L., "Enhancement of WIND-US for Helicopter Flow Simulation," 36th Fluid Dynamics Conference and Exhibit, AIAA Paper No. 2006-3373, San Francisco, CA, 5–8 June 2006.

[21] Chen, C. L., Chen, Y. C., Chen, B., Jain, R. K., Lund, T., Zhao, H., Wang, Z. J., Sun, Y., Saberi, H., and Shih, T. H., "High Fidelity Multidisciplinary Tool Development for Helicopter Quieting," 37th Fluid Dynamics Conference and Exhibit, AIAA Paper 2007-3807, Miami, FL, 25–28 June 2007.

[22] Saberi, H., Khoshlahjeh, M., Ormiston, R. A., and Rutkowski, M. J., "Overview of RCAS and Application to Advanced Rotorcraft Problems," American Helicopter Society 4th Decennial Specialist's Conference on Aeromechanics, San Francisco, CA, Jan. 2004.

[23] Potsdam, M., Yeo, H., and Johnson, W., "Rotor Airloads Prediction Using Loose Aerodynamic/Structural Coupling," *Journal of Aircraft*, Vol. 43, No. 3, May–June 2006, pp. 732–742.

[24] Nygaard, T. A., Saberi, H. A., Ormiston, R. A., Strawn, R. C., and Potsdam, M., "CFD and CSD Coupling Algorithms and Fluid Structure Interface for Rotorcraft Aeromechanics in Steady and Transient Flight Conditions," *American Helicopter Society 62nd Annual Forum Proceedings*, Phoenix, AZ, 9–11 May 2006.

[25] Tung, C., Cardonna, F. X., and Johnson, W. R., "The Prediction of Transonic Flows on an Advancing Rotor," *Journal of the American Helicopter Society*, Vol. 31, No. 3, July 1986, pp. 4–9.

[26] Ho, J. C., Yeo, H., and Ormiston, R. A., "Investigation of Rotor Blade Structural Dynamics and Modeling Based on Measured Airloads," *Journal of Aircraft*, Vol. 45, No. 5, Sept.–Oct. 2008, pp. 1631–1642. doi:10.2514/1.34025

[27] Yeo, H., Bousman, W. G., and Johnson, W., "Performance Analysis of a Utility Helicopter with Standard and Advanced Rotor," *Journal of the American Helicopter Society*, Vol. 49, No. 3, July 2004, pp. 250–270. doi:10.4050/JAHS.49.250

[28] Johnson, W., *Helicopter Theory*, Princeton Univ. Press, Princeton, NJ, 1980, pp. 288–289.

[29] Datta, A., and Chopra, I., "Validation of Structural and Aerodynamic Modeling Using UH-60A Airloads Program Data," *Journal of the American Helicopter Society*, Vol. 51, No. 1, Jan. 2006, pp. 43–57. doi:10.4050/1.3092877